Coupling between vesicle shape and lateral distribution of mobile membrane inclusions

Bojan Božič,[1,*] Veronika Kralj-Iglič,[1] and Saša Svetina[1,2]
[1]*Institute of Biophysics, Faculty of Medicine, University of Ljubljana, Lipičeva 2, SI-1000 Ljubljana, Slovenia*
[2]*Jožef Stefan Institute, Jamova 39, SI-1000 Ljubljana, Slovenia*
(Received 26 October 2005; revised manuscript received 6 February 2006; published 13 April 2006)

Membrane inclusions such as membrane-embedded peptides or proteins exhibit a curvature-dependent interaction with the surrounding lipid matrix due to the mismatch between their intrinsic curvature and the local membrane curvature. This interaction causes an inhomogeneous lateral distribution of the inclusions and a corresponding adjustment of the vesicle shape. We have studied theoretically the axisymmetric equilibrium shapes of lipid vesicles with mobile inclusions, taking into account that the membrane free energy includes the elastic energy of the lipid bilayer and a contribution due to an inclusion-membrane interaction. Equations describing the shape are derived by minimizing the total free energy at fixed membrane area, enclosed volume, and number of inclusions and are then solved numerically. It is shown that vesicle shape may assume a symmetry that differs from that of the vesicle with no inclusions. If the inclusion-membrane interaction exceeds a certain value, there is no axisymmetric solution of the equations with a continuous and derivable lateral density of inclusions over the whole area of the vesicle. When approaching the critical vesicle shape, the shapes obtained differ qualitatively from those described by the area difference elasticity model of the elastic properties of lipid membranes. In general, vesicle shapes adjust to the presence of inclusions by increasing regions with favorable curvature and decreasing regions of unfavorable curvature in a way such that the lateral distribution of inclusions becomes inhomogeneous.

DOI: 10.1103/PhysRevE.73.041915 PACS number(s): 87.16.Dg, 87.15.Kg, 83.10.Ff

I. INTRODUCTION

Biological membranes are multicomponent entities comprising a lipid matrix decorated by embedded and attached proteins and protein complexes. The essential element of many cellular processes such as intracellular protein transport [1], vesicle formation [2], and the establishment of cellular polarity [3] is the compositional variation over the membrane area. Most of such processes are also accompanied by changes of membrane conformation, which implies a coupling between cellular or organelle shapes and membrane lateral organization [4,5]. The physicochemical basis of these phenomena can be understood by studying simpler membrane systems. Studies of vesicles whose membranes are composed of a single lipid species, for instance, helped in understanding the essential aspects of the elasticity of liquid membranes that determine lipid vesicle shape (reviewed in [6]). Theoretical and experimental studies of membranes at the next higher level of complexity—i.e., membranes composed of binary mixtures—already showed the coupling between vesicle shapes and lateral distribution of membrane components and the complexity of the problem. This subject has been reviewed in a recent work of Harden *et al.* [7].

An example of a relatively simple binary membrane system that allows for a strict theoretical approach is the single lipid membrane with embedded, laterally mobile, membrane inclusions [8]. Such inclusions can be any membrane constituting molecule or any assembly of molecules distinct from the surrounding lipid matrix. In such a simplified binary system the lipid molecules that are not forming the inclusion can be treated as a continuum and the effect of inclusions on the state of a lipid vesicle as a modification of its behavior in their absence. Studies of membrane inclusions have focused on the strength of the interaction between an inclusion and its lipid environment [8,9], the effect of the inclusion-lipid matrix interaction on the membrane curvature [10], and the consequent indirect interaction between two inclusions [11]. Here we are interested in the influence of the inclusion-lipid interaction on the collective effect of all vesicle membrane inclusions on its shape. The idea is followed [12] that the equilibrium vesicle shape corresponds to the minimum of the sum of the energy contributions to the membrane energy that include elastic energy of the lipid matrix and free energy of inclusions, allowing for the lateral distribution of inclusions to be inhomogeneous due to the curvature dependent inclusion-lipid matrix interaction. Namely, laterally mobile inclusions are expected to move from regions of unfavorable curvature and to accumulate in regions of favorable curvature. By employing a parametric model of the vesicle shape it has been demonstrated [5,13] that the inclusion-curvature interaction causes a modification of the shape involving enhanced regions of favorable curvature and diminished regions of unfavorable curvature, thereby showing the coupling between the lateral density of the membrane inclusions and the vesicle shape.

The use of parametric models for vesicle shape determinations may lead to the omission of some important details and even qualitative features in the behavior of the system. In view of this, it is our purpose here to develop a rigorous, self-consistent variational approach to determine vesicle shape and the corresponding lateral distribution of inclusions, based on two contributions to the system free energy: the energy of the membrane bending and the free energy of the inclusions. The variational approach will be a generali-

*Electronic address: bojan.bozic@biofiz.mf.uni-lj.si

zation of the theoretical work on shapes of lipid vesicles with no inclusions. In the absence of inclusions the shapes are usually described by the area difference elasticity (ADE) model, in which the membrane bending energy consists of the local and nonlocal bending energy terms [14]. Methods for determining of equilibrium axisymmetric shapes based on minimization of the bending energy of a thin membrane under the constraints imposed by vesicle geometry are well developed [15]. In order to apply them to the membrane with inclusions, we generate an analytical expression for the free energy of this membrane by including an expression based on a membrane-curvature-dependent, single-inclusion energy and by applying methods of statistical physics considering the lateral distribution of inclusions [13,16,17].

The outline of the paper is as follows. In the section on theory (Sec. II) we shall first define the inclusion-membrane interaction for isotropic inclusions and the corresponding free energy of inclusions. Then we shall state the variational problem of minimization of the free energy of the membrane by a system of Euler-Lagrange differential equations. The problem will be solved numerically for few typical examples presented in the Results section (Sec. III). Previous work indicated that it is possible, by suitable expansions, to reduce the free energy of the membrane with inclusions to the ADE model with effective values of model parameters. Because there are indications that, in the attained equilibrium shape, the inclusions distribute in vesicle regions with membrane curvatures that are favorable for the inclusions in a manner different from that predicted by the ADE model [13], part of the Results section will be devoted to analysis of the validity of the ADE approximation. In the Discussion (Sec. IV) we concentrate on the specific results obtained by the rigorous approach to the solution of the problem.

II. THEORY

A. Basic properties of the model

The components of the model are bending elastic energies of the lipid bilayer and a term describing the free energy of inclusions. We shall first define the latter and then present the consequent expression of the membrane free energy. While the derivation of the free energy of the inclusions is given in detail elsewhere [17,18], only a brief description is given here: the free energy of inclusions derives from the single-inclusion energy that is based on the mismatch between the local curvature preferred by an inclusion and the actual local curvature of the membrane at the site of the inclusion.

Local membrane curvature is described by two principal curvatures that we denote as C_1 and C_2. The intrinsic shape of the inclusion can be described by its characteristic principal curvatures $C_{1\mathrm{m}}$ and $C_{2\mathrm{m}}$. The inclusions are defined as point inclusions, meaning that their contribution to the membrane area is negligible. The single-inclusion energy has been derived previously [16,18]. In this work we shall restrict ourselves to isotropic inclusions for which their principal curvatures are equal to the mean inclusion curvature (H_m), $C_{1\mathrm{m}}=C_{2\mathrm{m}}=H_\mathrm{m}$. In this approximation the expression for the single-inclusion energy reads

$$E=\frac{\xi}{2}(H-H_\mathrm{m})^2+\frac{\xi+\xi^*}{16}(C_1-C_2)^2, \tag{1}$$

where ξ and ξ^* are the interaction constants that express the strength of interaction and

$$H=\frac{1}{2}(C_1+C_2) \tag{2}$$

is the mean curvature.

For any shape of a vesicle that differs from a sphere, principal curvatures vary over the vesicle surface. Consequently, due to the interaction term [Eq. (1)] and according to statistical physics, inclusions distribute over the membrane in a laterally inhomogeneous manner as [13]

$$m=\frac{m_\mathrm{u}e^{-E/k_\mathrm{B}T}}{\frac{1}{A}\int e^{-E/k_\mathrm{B}T}dA}, \tag{3}$$

where m is the lateral density and m_u is the mean lateral density of inclusions, k_B is the Boltzmann constant, and T is the temperature. The integration is over the whole membrane area A. The corresponding free energy, expressed as a deviation from the free energy for a laterally homogeneous case, is [13]

$$F_\mathrm{m}=\int m\left(E+k_\mathrm{B}T\ln\frac{m}{m_\mathrm{u}}\right)dA. \tag{4}$$

The total free energy of the phospholipid membrane with inclusions (F) then consists of two respective contributions,

$$F=F_\mathrm{m}+F_\mathrm{PC}, \tag{5}$$

where F_m is the contribution of the inclusions and F_PC is the free energy of the deformation of the phospholipid continuum which, in the ADE model, is expressed as [14]

$$F_\mathrm{PC}=\frac{k_\mathrm{c}}{2}\int(2H-C_0)^2dA+k_\mathrm{G}\int C_1C_2dA+\frac{k_\mathrm{r}}{2D^2A}(\Delta A-\Delta A_0)^2, \tag{6}$$

where k_c is the bending constant, k_G the Gaussian bending constant, k_r the nonlocal bending constant, C_0 the spontaneous curvature of the membrane, D the distance between the neutral surfaces of the two membrane leaflets,

$$\Delta A=2D\int HdA \tag{7}$$

the difference between the areas of the two membrane leaflets, and ΔA_0 the difference between their equilibrium areas. As we will consider only closed shapes, we will omit the Gaussian term in Eq. (6), since it is constant for closed shapes.

B. Minimization of the membrane free energy

The equilibrium configuration of the system is given by the membrane shape and the density of the inclusions, which

give minimal free energy under relevant constraints. We require the membrane area (A), the enclosed volume (V), and the number of inclusions in the membrane ($N_T=m_uA$) to be constant.

For clarity, the above problem is expressed in dimensionless form. We introduce dimensionless quantities

$$c_1 = R_s C_1, \quad c_2 = R_s C_2, \quad c_0 = R_s C_0, \quad h_m = R_s H_m \tag{8}$$

and

$$da = \frac{dA}{4\pi R_s^2}, \tag{9}$$

where the normalization unit R_s is the radius of the sphere of the membrane area A ($R_s=\sqrt{A/4\pi}$). For simplicity, we take $\xi=\xi^*$ and, for clarity, we introduce a relative lateral density of the inclusions ν ($\nu=m/m_u$), a dimensionless interaction constant κ ($\kappa=\xi/k_BTR_s^2$), and a dimensionless constant p measuring the total number of inclusions ($p=N_Tk_BT/8\pi k_c$). Dividing the free energy (F) by the bending energy of a sphere ($8\pi k_c$) yields the relative free energy

$$f = p\int \nu\left(\frac{\kappa}{8}(c_1+c_2-2h_m)^2 + \frac{\kappa}{8}(c_1-c_2)^2 + \ln\nu\right)da + \frac{1}{4}\int (c_1+c_2-c_0)^2 da + \frac{k_r}{k_c}(\Delta a-\Delta a_0)^2, \tag{10}$$

where $\Delta a=\Delta A/8\pi R_sD$ and $\Delta a_0=\Delta A_0/8\pi R_sD$, with $8\pi R_sD$ the difference between the areas of the two membrane leaflets of a sphere of radius R_s. The first term in Eq. (10) represents the relative free energy of inclusions (f_m) whereas the second and third represent the relative bending (w_b) and the relative nonlocal bending energy (w_{RE}), respectively.

The extremes of f correspond to the stationary points of the functional

$$g = f - \lambda_a(a-a_0) - \lambda_v(v-v_0) - \lambda_\nu(n-n_0), \tag{11}$$

where the relative membrane area ($a=A/4\pi R_s^2$), the relative volume ($v=3V/4\pi R_s^3$), and the relative number of inclusions in the membrane ($n=N_T/N_{T0}$) are fixed. From the definitions of the relative membrane area and the relative number of inclusions it follows that $a_0=1$ and $n_0=1$. The constraints regarding the volume, the membrane area, and the number of inclusions are incorporated in free energy minimization by introducing the Lagrange multipliers λ_v, λ_a, and λ_ν. In the stationary point, the variation of the functional [Eq. (11)] with respect to arbitrary configuration deviation is zero. Written out, the variation of g is

$$\delta g = \delta f_m + \delta w_b + \delta w_{RE} - \lambda_a\delta a - \lambda_v\delta v - \lambda_\nu\delta n, \tag{12}$$

where the variation of the nonlocal bending energy (δw_{RE}) can be expressed by $\lambda_{\Delta a}\delta\Delta a$ where

$$\lambda_{\Delta a} = 2\frac{k_r}{k_c}(\Delta a-\Delta a_0). \tag{13}$$

We restrict ourselves to the axisymmetric shapes. Therefore, the principal curvatures—the relative parallel curvature (c_p) and the relative meridian curvature (c_m)—can be written in the form $c_p=\sin\psi/\rho$, $c_m=\dot{\psi}$, where ψ is the angle between the symmetry axis and the normal to the membrane contour, ρ is the distance between the symmetry axis and a certain point on the contour normalized to R_s, and the overdot denotes the derivative with respect to the arclength (l) that is normalized to R_s. Using the expressions for the relative membrane area $a=\frac{1}{2}\int\rho dl$, the relative volume $v=\frac{3}{4}\int\rho^2\sin\psi dl$, the relative difference between the monolayer areas $\Delta a=\frac{1}{4}\int(\sin\psi+\rho\dot{\psi})dl$, and the relative number of inclusions $n=\frac{1}{2}\int\nu\rho dl$, we can express the variation of the functional g as

$$\delta g = \delta\int \mathcal{L}dl, \tag{14}$$

where the Lagrangian function is written as

$$\mathcal{L} = \kappa p\frac{\rho\nu}{16}\left[\left(\frac{\sin\psi}{\rho}+\dot{\psi}-2h_m\right)^2+\left(\frac{\sin\psi}{\rho}-\dot{\psi}\right)^2\right] + p\frac{\rho}{2}\nu\ln\nu + \frac{\rho}{8}\left(\frac{\sin\psi}{\rho}+\dot{\psi}-c_0\right)^2 - \lambda_a\frac{\rho}{2} - \lambda_v\frac{3}{4}\rho^2\sin\psi - \lambda_{\Delta a}\frac{1}{4}(\rho\dot{\psi}+\sin\psi) - \lambda_\nu\frac{\rho\nu}{2} + \lambda(\dot{\rho}-\cos\psi). \tag{15}$$

The restriction of the geometrical relation between the variables ρ and ψ ($\dot{\rho}=\cos\psi$) is taken into consideration by the local Lagrange multiplier [$\lambda=\lambda(l)$].

The variation of the functional with respect to the shape is zero ($\delta g=0$) if the Euler-Lagrange equations

$$\frac{\partial\mathcal{L}}{\partial\rho} - \frac{d}{dl}\left(\frac{\partial\mathcal{L}}{\partial\dot{\rho}}\right) = 0, \tag{16}$$

$$\frac{\partial\mathcal{L}}{\partial\psi} - \frac{d}{dl}\left(\frac{\partial\mathcal{L}}{\partial\dot{\psi}}\right) = 0 \tag{17}$$

and

$$\frac{\partial\mathcal{L}}{\partial\nu} = 0 \tag{18}$$

are fulfilled. Using expression (15) and the definition $\chi=\rho\dot{\psi}$, the Euler-Lagrange equations give system of equations in the form $\dot{\lambda}=\dot{\lambda}(\rho,\psi,\chi,\nu)$, $\dot{\chi}=\dot{\chi}(\rho,\psi,\chi,\lambda,\nu,\dot{\nu})$, and

$$\ln\nu = -1 + \frac{\lambda_\nu}{p} - \frac{\kappa}{8}\left[\left(\frac{\sin\psi}{\rho}+\frac{\chi}{\rho}-2h_m\right)^2+\left(\frac{\sin\psi}{\rho}-\frac{\chi}{\rho}\right)^2\right]. \tag{19}$$

For solving this system of equations, it is convenient to eliminate $\dot{\nu}$ in the expression for $\dot{\chi}$. This is done by first differentiating Eq. (19) with respect to l,

$$\frac{d\nu}{dl} = -\frac{\kappa\nu}{2}\left(\frac{d\chi}{dl}\frac{1}{\rho^2}(\chi - h_m\rho) + \frac{\cos\psi}{\rho^3}(\chi\sin\psi + h_m\rho\sin\psi - \sin^2\psi - \chi^2)\right) \quad (20)$$

and then inserting expression (20) into the expression for $\dot{\chi}$, which gives the equation

$$\frac{d\chi}{dl}\left(1 + \kappa p\nu - \frac{\kappa^2 p\nu}{2\rho^2}(\chi - h_m\rho)^2\right) = \frac{\sin\psi\cos\psi}{\rho}\left(1 + \kappa p\nu + \frac{\kappa^2 p\nu}{2\rho^2}(\chi^2 - h_m^2\rho^2)\right) - 3\lambda_v\cos\psi\rho^2 + 4\lambda\sin\psi - \frac{\kappa^2 p\nu\cos\psi}{2\rho^3}(\chi - h_m\rho)(\sin^2\psi + \chi^2). \quad (21)$$

Written out, the equation for $\dot{\lambda}$ is

$$\frac{d\lambda}{dl} = \frac{1}{8}\frac{(\chi - c_0\rho)^2 - \sin^2\psi}{\rho^2} + \frac{\kappa p\nu}{8}\left(\frac{\chi^2 - \sin^2\psi}{\rho^2} - 2h_m\frac{\chi}{\rho} + 2h_m^2\right) + \frac{p}{2}\nu\ln\nu - \frac{\lambda_a}{2} - \frac{3\lambda_v}{2}\rho\sin\psi - \frac{\lambda_{\Delta a}}{4}\frac{\chi}{\rho} - \frac{\lambda_\nu}{2}\nu. \quad (22)$$

The system of differential equations [Eqs. (21) and (22)] is solved numerically by considering the expression for the density of inclusions [Eq. (19)]. In the procedure, the initial values of the curvatures of both poles and of the Lagrange coefficients (λ_v, λ_a, $\lambda_{\Delta a}$, and λ_ν) are chosen. At the poles, the parallel and meridian curvatures are equal, and λ equals zero because the shape of the membrane has to be smooth. The integration over the arclength l is performed from both poles. The position along the symmetry axis (z) is obtained by using the geometrical relation between z and ψ ($\dot{z} = -\sin\psi$). Both integrations are stopped at the relative area 0.5 so that the relative area of the whole calculated shape is equal to 1. Then, the validity of the constraints given by the volume, the difference between the equilibrium areas of the monolayers[1] and the number of the inclusions, and the continuity of ρ, c_p and c_m at the joining point are tested, and new initial values of the above six quantities are set. The procedure is iterated until the constraints and continuity of the variables are fulfilled up to a prescribed accuracy. It can be seen from Eq. (19) that the requirement for the continuity of ν at the joining point is automatically fulfilled by taking into consideration the continuity of ρ, c_p, and c_m.

[1]Numerically calculated difference between the equilibrium areas of the monolayers ($\Delta a_{0,num}$) is obtained from numerically calculated difference between the areas of the monolayers (Δa_{num}) by using Eq. (13), $\Delta a_{0,num} = \Delta a_{num} - k_c\lambda_{\Delta a}/2k_r$.

C. Limit of small single-inclusion energy

Since for many shapes the principal curvatures are small all over the membrane, it is convenient to study the shape configurations in the limit of small, single-inclusion energy. At equilibrium the free energy of the inclusions [Eq. (4)] can be expressed also as [13]

$$F_{m,equ} = -k_B T N_T \ln\left(\frac{1}{A}\int e^{-E/k_B T} dA\right). \quad (23)$$

If the single-inclusion energy (E) is small in comparison to $k_B T$ all over the surface, we can expand the exponential and logarithmic function of the expression (23) into a series. Up to the second order in $E/k_B T$ we obtain the equilibrium free energy of the inclusions [13] in the form

$$F_{m,equ} \approx k_B T N_T \int\left[\frac{E}{k_B T} - \frac{1}{2}\left(\frac{E}{k_B T}\right)^2\right] dA + \frac{k_B T N_T}{2}\left(\int\frac{E}{k_B T} dA\right)^2. \quad (24)$$

Though the single-inclusion energy is small, $F_{m,equ}$ can be large since it is proportional to the number of inclusions.

By inserting expression (1) into expression (24), we obtain the free energy $F_{m,equ}$ expressed explicitly by the principal curvatures and the intrinsic inclusion curvature. At large inclusion curvatures the single-inclusion energy can also be small in comparison to $k_B T$ in some regions of the vesicle surface if large principal curvatures are fit for the inclusion curvature. However, the single-inclusion energy can be small all over the vesicle surface only at small principal curvatures and at small intrinsic inclusion curvatures. By taking into consideration the assumption of small single-inclusion energy all over the vesicle surface, from expression (1) we obtain the condition for the inclusion curvature $H_m^2 \ll 2k_B T/\xi$ and for the principal curvatures

$$C_1^2 \ll \frac{8k_B T}{\xi}, \quad C_2^2 \ll \frac{8k_B T}{\xi}. \quad (25)$$

According to Eqs. (25), in the expression for the equilibrium free energy we can retain only terms up to the second order in the principal curvatures. By incorporating the inclusion energy terms in the expression of the ADE model, the free energy is

$$F_{equ} = \frac{1}{2}k_{c,eff}\int(C_1 + C_2 - C_{0,eff})^2 dA + \frac{k_{r,eff}}{2D^2 A}(\Delta A - \Delta A_{0,eff})^2, \quad (26)$$

where we have omitted terms that are constant for closed shapes. The effective coefficients of the ADE model are

$$k_{c,eff} = k_c(1 + \xi m_u/2k_c - H_m^2\xi^2 m_u/4k_B T k_c),$$

$$C_{0,eff} = (C_0 + H_m\xi m_u/2k_c)/(1 + \xi m_u/2k_c - H_m^2\xi^2 m_u/4k_B T k_c),$$

$$k_{r,eff} = k_r + H_m^2\xi^2 m_u/4k_B T,$$

and

$$\Delta A_{0,\mathrm{eff}} = \Delta A_0/(1 + H_\mathrm{m}^2 \xi^2 m_\mathrm{u}/4k_\mathrm{B}Tk_\mathrm{r}).$$

Within the limit of small single-inclusion energy the set of possible vesicle shapes is the same as for the ADE model.

D. Estimation of model constants

The membrane free energy and the corresponding Euler-Lagrange differential equations are subject to constants that express the characteristics of the inclusions and of the membrane. It can be estimated that ξ is roughly no greater than 10^{-30} J m^2 [16,19], and we have taken into consideration that the intrinsic curvature of inclusions (H_m) does not exceed 10^7 m^{-1} [19]. For a phospholipid vesicle with radius R_s of 10 μm, we take the number of inclusions (N_T) to be no greater than 10^6. The membrane bending constant (k_c) is taken to be 10^{-19} J [20] and the ratio between the local and the nonlocal bending constants ($k_\mathrm{r}/k_\mathrm{c}$) to be 3 [21].

For $H_\mathrm{m} \approx 0$, the criterion of small single-inclusion energy coincides with Eqs. (25). For $R_\mathrm{s}=10$ μm, it follows that $8/\kappa \approx 10^4$ so that the criterion of small single-inclusion energy is fulfilled all over the vesicle surface, other than for shapes that exhibit a neck radius smaller than 1 μm.

III. RESULTS

A. Effects of inclusions on the shape symmetry

The equilibrium shape and the corresponding lateral density of inclusions were calculated numerically. The calculations show that the inclusions can significantly change the shape of the vesicles. Here, we focus on the mutual effect between the shape of the membrane and the lateral density distribution of inclusions. The fact that the inclusions may cause transitions between different shape classes [13] has also been considered. We present the result for a typical case of shape transition caused by increasing the number of inclusions when the initial shape corresponds to the minimal free energy of the phospholipid continuum [Eq. (6)].

In Fig. 1 the vesicle characteristics are presented as a function of the number of inclusions for the oblate shape that is asymmetric with respect to the equatorial plane. The inclusions were chosen to prefer positive mean curvature ($H_\mathrm{m}>0$) of the membrane [Eq. (2)]. In Fig. 1(a) we can see how the number of inclusions affects the vesicle shape and the relative lateral density of inclusions. The variation of the latter is relatively small all over the membrane for all shapes. At smaller number of inclusions (shapes *A* and *B*), two regions of practically constant density are seen. In the region of the invaginated part of the vesicle the density is lower than in the region where the mean curvature is positive, which is the consequence of the chosen positive H_m. At a higher number of inclusions the effect on the shape is more pronounced. The difference between the areas of the bilayer leaflets [Eq. (7)] increases with increasing inclusion number until a discontinuous shape transition to the symmetric shape, with respect to the equatorial plane, takes place [Fig. 1(b)]. Near the vesicle equator these symmetric shapes have a slightly higher density of inclusions than the mean density.

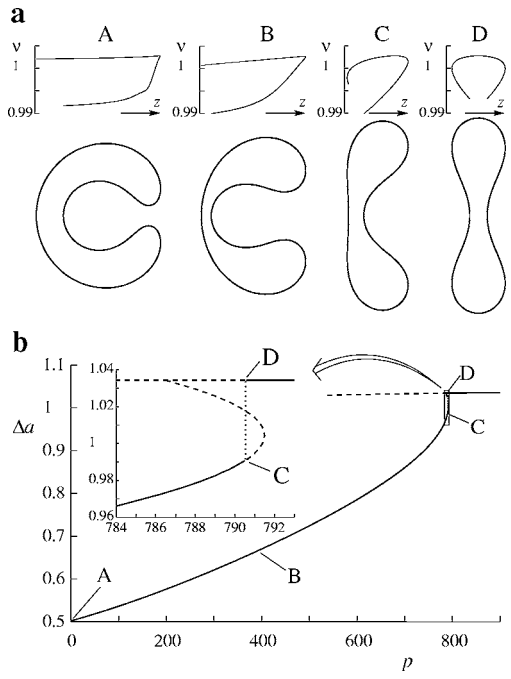

FIG. 1. The dependences of the vesicle shape, the inclusion lateral density, and the difference between the areas of membrane monolayers on the number of inclusions (N_T) for a relative volume (v) equal to 0.6, κ to 10^{-4}, h_m to 30, c_0 to 0, Δa_0 to 0.5022, and k_r/k_c equal to 3. The number of inclusions is expressed by the parameter p, where $p=k_\mathrm{B}TN_\mathrm{T}/8\pi k_\mathrm{c}$. The initial shape at $N_\mathrm{T}=0$ corresponds to the minimal elastic energy where $\Delta a=\Delta a_0$. (a) The axial cross sections of the shapes for values of p equal to 1 for shape *A*, 395 for shape *B*, and 790.5 for the shapes *C* and *D*. The relative inclusion density (ν) is also presented above the shape contours. (b) The relative difference between the areas of membrane monolayers (Δa) as a function of p. Solid parts of the lines denote stable configurations, and dashed parts denote unstable configurations. The dotted vertical line shows the occurrence of the discontinuous shape transitions. The points marked by *A*, *B*, *C* and *D* show the locations of shapes presented. The inset shows an enlarged marked region of the discontinuous shape transition.

One can pose the question as to why the inclusions prefer symmetric shapes with respect to the equator. The vesicle assumes a shape that involves preferentially those parts of the membrane with larger mean curvature, which is energetically more favorable. The symmetric shapes (cf. case *D* in Fig. 1) have regions of relatively large mean membrane curvature in the vicinity of the equator and do not have regions of large negative membrane curvature in the vicinity of a single pole as do asymmetric shapes.

B. Occurrence of a critical shape

It can be seen from Eq. (21) that the expression inside the parentheses on the left-hand-side of the equation takes the value 0 if the values of the constants κ and p are sufficiently high. Consequently, there is a singularity in the equation for $\mathrm{d}\chi/\mathrm{d}l$ which is also reflected in the singularity in $\mathrm{d}\nu/\mathrm{d}l$ as can be seen from Eq. (20). Caution was therefore needed in numerically solving the system of differential equations. It

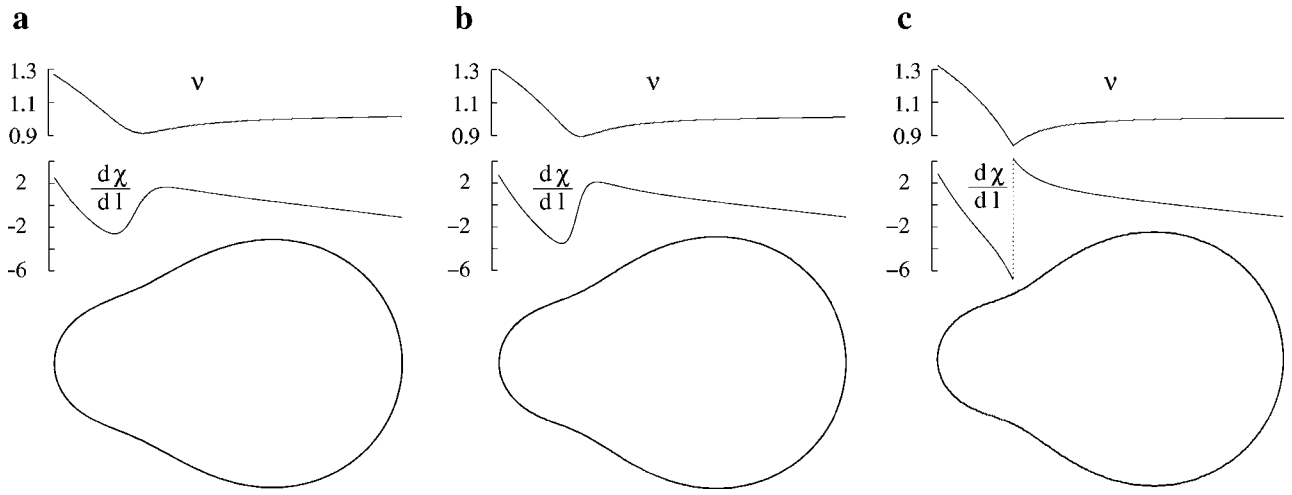

FIG. 2. Vesicle configurations at the approach to the critical shape. The lateral density of the inclusions (ν), the derivative $d\chi/dl$, and the corresponding shape are shown for three different values of the relative area difference (Δa): 1.02837 (a), 1.03037 (b), and 1.032375 (c). The values of other model parameters are $v=0.95$, $c_0=0$, $h_m=15$, $p=150$, and $\kappa=0.012$. The configurations were obtained by solving Eqs. (19), (21), and (22).

cannot be known in advance where along the contour the singularity will appear. By increasing the constants κ and p or varying geometrical constraints, we can approach the shape in which the singularity first appears at one point along the contour (representing a ring on the axisymmetric shape). We call such a shape a critical shape.

Convenient shapes for the study of the singularity are the pear shapes [4,22] in which the singularity is attained in the region of negative meridian curvature where the principal curvatures change significantly. Figure 2 illustrates how the critical shape is approached as Δa is increased.[2] A sequence of shapes for three different values of the area difference Δa is shown where the last shape [Fig. 2(c)] corresponds to the critical shape. The lateral density of the inclusions (ν) and the derivative $d\chi/dl$ are also shown. It can be seen in Fig. 2(a) that the density ν varies smoothly over the contour. There is an increase of the lateral density of the inclusions towards the pole that exhibits larger principal curvatures, since the intrinsic mean curvature of the inclusions is larger than any mean curvature attained on the equilibrium shape. In Fig. 2(b), the increase in density ν is more pronounced towards the left pole than in the shape shown in Fig. 2(a). In Fig. 2(c), this effect is still stronger. Correspondingly, the derivative $d\chi/dl$ varies smoothly and attains lower minimum values in Fig. 2(b) than in Fig. 2(a), while in Fig. 2(c) there is a discontinuous change in $d\chi/dl$ and the difference between the maximum and minimum values of $d\chi/dl$ is the largest. At first sight, all three shapes appear to be almost the same. However, a closer look reveals that, closer to the critical shape, a dip on the contour, corresponding to the strong changing of ν, becomes more pronounced when the critical shape is approached. Also the principal curvatures vary smoothly until the critical shape is reached. Figure 3 further illustrates the behavior of the system for the critical shape. Additional functions are shown: both principal curvatures, the derivative of the density $d\nu/dl$, and the numerator and denominator of the differential equation for $d\chi/dl$ [Eq. (21)]. Figure 3 shows that both the numerator and denominator of the critical shape approach zero linearly in the vicinity of the singularity.

To solve the system of differential equations for the critical shape, it is necessary to demonstrate the shape behavior in the vicinity of the singularity point for the critical shape. Extrapolation of the results towards the critical shape indicated that the numerator and denominator of the expression for $d\chi/dl$ [see Eq. (21)] attain zero values at the same point. Otherwise, for all the shapes considered, the denominator was always positive. In the vicinity of the singularity point the system of equations is solved in the form of an expansion

$$\rho = \rho_0 + \rho_1 l, \quad \psi = \psi_0 + \psi_1 l, \quad \chi = \chi_0 + \chi_1 l,$$

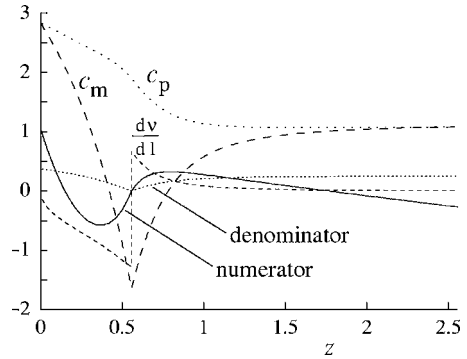

FIG. 3. The principal curvatures c_p and c_m, the derivative of the inclusion density $d\nu/dl$, and the numerator and denominator of the expression for $d\chi/dl$ [Eq. (21)] for the critical shape whose parameters correspond to the shape (c) in Fig. 2.

[2]The calculation of shapes for given Δa is similar to the calculation of shapes for given Δa_0. In the first case the constraint in Δa is taken into consideration by additional Lagrange multiplicator. The variation of the corresponding free energy leads to the equal system of differential equations as in the latter case.

$$\lambda = \lambda_0 + \lambda_1 l, \quad \nu = \nu_0 + \nu_1 l, \tag{27}$$

where ρ_0, ψ_0, χ_0, λ_0, and ν_0 correspond to the singularity point and ρ_1, ψ_1, χ_1, λ_1, and ν_1 denote the derivatives. Substituting Eqs. (27) into Eqs. (20)–(22) and neglecting nonlinear terms, we obtain the system of equations

$$\nu_1 = C_{\nu,\chi}\chi_1 + C_{\nu,0}, \tag{28}$$

$$\chi_1 = \frac{C_{\mathrm{num},\rho}\rho_1 + C_{\mathrm{num},\psi}\psi_1 + C_{\mathrm{num},\chi}\chi_1 + C_{\mathrm{num},\lambda}\lambda_1 + C_{\mathrm{num},\nu}\nu_1}{C_{\mathrm{de},\rho}\rho_1 + C_{\mathrm{de},\chi}\chi_1 + C_{\mathrm{de},\nu}\nu_1}, \tag{29}$$

$$\lambda_1 = C_{\lambda,0}, \tag{30}$$

where coefficients (C_i) depend only on ρ_0, ψ_0, χ_0, λ_0, and ν_0. Additionally, using the geometrical relation between ρ and ψ and the definition for χ, we obtain

$$\rho_1 = \cos\psi_0, \tag{31}$$

$$\psi_1 = \frac{\chi_0}{\rho_0}. \tag{32}$$

The derivatives of ρ, ψ, and λ with respect to arclength are the same on both sides of the singularity point, which is demonstrated by Eqs. (30)–(32). However, the combination of Eqs. (28)–(32) demonstrates that there are two different solutions for the derivatives of χ and ν. The singularity thus consists in the discontinuity of these two derivatives. Furthermore, the abrupt changes of the functions $d\chi/dl$ and $d\nu/dl$ at the singularity point are proportional to each other because of the linear relationship between χ_1 and ν_1 [cf. Eq. (28)].

C. Deviation from the expansion

The purpose of this subsection is to illustrate that under some conditions the expansion of the membrane free energy yielding the ADE model [Eq. (26)] is satisfactory, but that there are conditions where the system behavior that this model predicts differs from that obtained exactly in a qualitatively different manner. We shall present different examples. In the case presented in Fig. 1 the ADE model with effective coefficients [Eq. (26)] approximates well the exact expression [Eq. (10)], because the value of dimensionless interaction constant is small. The two vesicle shapes pertaining to the approximate expression and to the exact expression of the free energy are almost indistinguishable.

The second example presents a comparison between the critical shape [Fig. 2(c)] which was obtained exactly and the shape obtained by the ADE model in which the parameters are the same as for the critical shape. The shape obtained by the ADE model is slightly elongated and the dip on the contour is smaller (Fig. 4). However, these two shapes look quite similar, in spite of the fact that in the treated case, due to the relatively large intrinsic inclusion curvature, the single-inclusion energy is actually not small in comparison to k_BT. The difference between the two solutions is even more apparent when we compare the corresponding inclusion densities. In Fig. 4 the inclusion densities correspond to the minimum of the free energy of inclusions [Eq. (4)] for each shape. It can be seen that the two inclusion lateral densities differ qualitatively, in that the lateral density of the approximate solution is smooth throughout the membrane surface, whereas the exact solution exhibits a discontinuity in the derivative of the inclusion density. Because the principal curvatures in the ADE model [Eq. (26)] are always smooth throughout the vesicle surface, this model can never predict the occurrence of the critical shape.

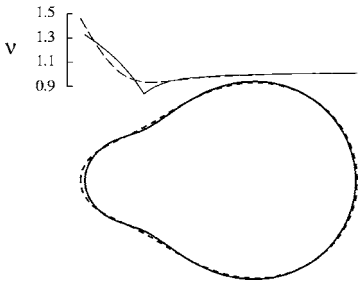

FIG. 4. Comparison between the configuration of the exact solution (solid lines) and the approximate one (dashed lines) by presenting the relative lateral densities of the inclusions (ν) and the corresponding shapes. The lateral densities are obtained using Eq. (3). The values of the parameters (Δa, v, c_0, h_m, p, and κ) for both configurations are the same as for the shape (c) in Fig. 2.

Another example of the qualitative difference between the exact solution and the one obtained by the ADE model will be demonstrated by considering the effect of the dimensionless interaction constant (κ) on the prolate (Fig. 5) and oblate (Fig. 6) vesicle shapes involving narrow necks. In both cases shapes are chosen for the analysis for which the nonlocal bending energy is zero at $\kappa=0$. For such shapes Δa equals Δa_0. The characteristic of these shapes is the particularly large principal curvatures at their neck and mouth regions, respectively. As a consequence, the single-inclusion energy can become very large in these regions, particularly at larger values of κ. The ADE model with effective coefficients predicts the behavior correctly only for small values of the interaction constant κ, in that the dependence of Δa on κ and the corresponding shapes are almost the same for the exact and approximative solutions (Figs. 5 and 6). For prolate shape and positive intrinsic curvature of the inclusions (Fig. 5), the difference between the areas of the membrane monolayers (Δa) increases at smaller κ values and the width of the neck decreases. Similarly, for oblate shape and negative intrinsic curvature (Fig. 6), Δa and the width of the mouth decrease at smaller κ. Further, at smaller values of κ the lateral density of inclusions is almost homogeneous over the whole surface, whereas at larger values the density in the vicinity of the neck (Fig. 5) and the mouth (Fig. 6) drastically decreases. The difference between the predictions of the exact and approximative solution appears when the energy of the single inclusion is no longer small all over the surface and, therefore, the membrane elastic energy cannot be well described by the ADE model with effective coefficients. The increase of Δa obtained by the exact solution is more steep than for the approximate one because vesicle shapes obtained by the exact solution are better adjusted to

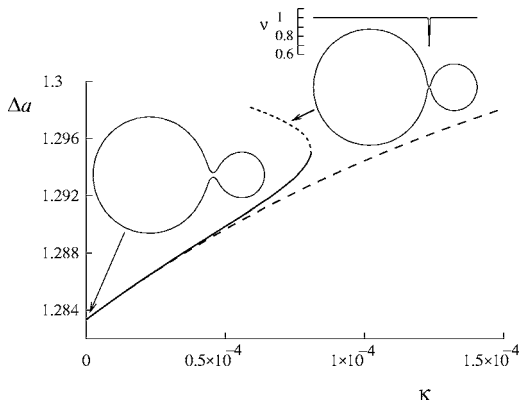

FIG. 5. The dependences of the difference between the areas of membrane monolayers (Δa) on the dimensionless interaction constant (κ) for the prolate shape of the relative volume (v) equal to 0.85, the constant p ($k_B T N_T / 8\pi k_c$) equal to 150, the relative intrinsic curvature of inclusions (h_m) equal to 30, the relative spontaneous curvature of membrane (c_0) equal to 3, the relative equilibrium difference between the areas of membrane monolayers (Δa_0) equal to 1.2833, and the ratio between the nonlocal and local bending constants (k_r/k_c) equal to 3. The line composed of the solid and dotted parts denotes Δa of shapes obtained by solving Eqs. (19), (21), and (22). It ends where we encountered numerical problems. The dashed line denotes Δa of shapes obtained within the ADE model. The axial cross sections of shapes at the indicated positions are given. For the shape with narrower neck the density ν is also presented.

the effect of the inclusions. In Fig. 5 the thinness of the neck can be explained by considering that the inclusions favor large positive curvature. The total free energy of inclusions [Eq. (4)] is smaller for the shape of smaller neck width that thus exhibits larger regions of positive mean curvature. Analogously, for the oblate shape (Fig. 6), the mouth is thin because of the negative intrinsic curvature of the inclusions.

For large values of κ there are two branches of shapes representing the exact solution. In the dependences of Δa on κ (Figs. 5 and 6), the dotted lines correspond to larger values and the solid lines to lower values of the free energy (f). On

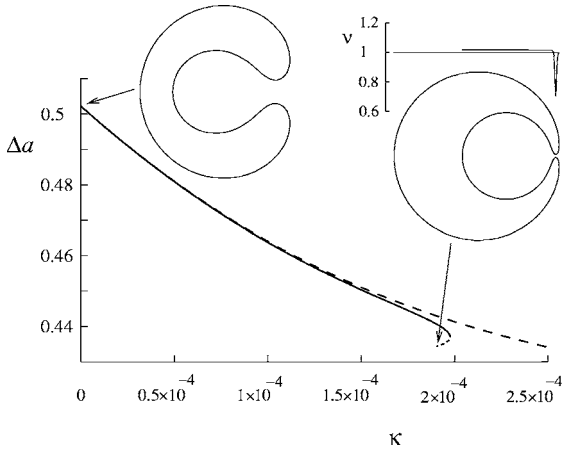

FIG. 6. The same as in Fig. 5 except the shape presented is oblate. Also values of the constants are the same as in Fig. 5 except $v=0.6$, $h_m=-30$, $c_0=0$, and $\Delta a_0=0.5022$.

the other hand, by the ADE model with effective coefficients, only one branch of shapes is predicted. The discrepancies in the vesicle shapes and in the lateral density of inclusions are more pronounced as the shapes with very narrow neck are approached.

Our calculations show that, at a given Δa, the difference between the respective shapes is negligible in the range where the corresponding values of κ significantly deviate. At larger values of κ, the lateral density in the vicinity of the neck and mouth drastically decreases, as does the lateral density pertaining to the exact shape. One can ask why there is so little difference in vesicle shape at a given Δa between the exact and approximate methods, even for large κ. This can be explained by the fact that the single-inclusion energy is large only in the small area in the neck or mouth region, where the density ν drops, and therefore the respective shapes at given Δa are almost the same.

IV. DISCUSSION

We have analyzed the effects of vesicle shape and lateral distribution of laterally mobile membrane inclusions on each other. Membrane inclusions—e.g., single species of peptides or proteins—were considered as embedded in the lipid matrix. Polymers attached at one side of the membrane could constitute an analogous system, with the same expected behavior [23]. These systems provide a relatively simple example of membranes composed of two components. Studies of the behavior of membranes with mixed composition are relevant because biological membranes are multicomponent membranes and because many biological processes depend on how these components distribute or even segregate laterally. Whereas the general treatment of binary mixtures usually requires the application of different approximations, the advantage of the model treated here, which is a special limiting case of binary mixture systems, is that its behavior can be studied in a rigorous manner, allowing for a detailed investigation of the model properties. On the other hand, this model does not contain features of binary mixtures such as the possible dependence of membrane mechanical constants on the local fractions of membrane components. In the following we shall, after discussing the model and methods of analysis, evaluate, on the basis of exact calculations, the applicability of the two approximate methods—i.e., the expansion of the free energy up to second order and the use of the parametric models. We shall then pay special attention to the features revealed by the rigorous approach and, in particular, discuss the reasons causing the occurrence of the critical shape.

The single-inclusion energy is defined as the consequence of the mismatch between local membrane curvature and the intrinsic shape of the inclusion. Due to the corresponding energy term, mobile inclusions distribute over the membrane according to Boltzmann statistics. As discussed earlier [13] this approach differs from models where a phenomenological coupling between the membrane curvature and the area densities of membrane constituents was applied according to a Ginzburg-Landau expansion method [10]. Essentially, it is based on the energy of the interaction of an individual em-

bedded molecule with the membrane curvature at the site of the molecule. The interaction term in this model is proportional to the square of the mean curvature whereas the Ginzburg-Landau expansion leads to the corresponding energy term that is proportional to the mean curvature.

We neglect the effects arising from direct interactions between inclusions. The effect that is associated with the solvent entropy density of the phospholipid molecules [24] is also not included. It can be estimated and compared to the effect that is associated with the inclusion entropy density given in our model by the second term in Eq. (4). The evaluation of the two entropy densities for the examples presented in the Results section gives the result that the solvent entropy is 10 times smaller than the inclusion entropy. In addition, the variation of the solvent entropy density over the membrane area is smaller than the corresponding variation of the inclusion entropy. The ratio between these entropy terms essentially depends on the density of inclusions. In our examples the largest values of this density are achieved in Fig. 1. We consider that the omission of the solvent entropy is acceptable.

We used the expression of the free energy for isotropic inclusions, added it to the membrane bending energies [12,13], and looked for the vesicle shape that corresponds to the minimum of the total free energy of the system. The system was restricted to the case of axially symmetric inclusions because, for simplicity, we decided not to include inclusion orientation as an additional degree of freedom [25]. Even with this simplification the inclusion-lipid matrix interaction still involves two independent energy terms measuring the deviation of the mean curvature from the intrinsic curvature of the inclusion and the effect due to the difference between the values of the two principal curvatures. The analysis was only performed for one value of the ratio between the two respective interaction constants ($\xi/\xi^{*}=1$) and therefore does not provide information about the relative influences of these two interaction terms. The focus of the analysis was rather on formulating the variational problem of minimization of the vesicle free energy. This problem was stated at relevant constraints, and the corresponding system of Euler-Lagrange differential equations was derived. The system of equations obtained [Eqs. (19), (21), and (22)] is a generalization of the Euler-Lagrange differential equations which have been used in vesicle shape determinations [15] in that, in addition to the variables defining vesicle shape, they involve as an additional variable the lateral density of the inclusion.

It has been shown for the free energy of the two component vesicles [26], and also for the system with inclusions [13], that under certain conditions it can be expressed in terms of the ADE model with effective model constants. We rederived this expansion for an arbitrary value of intrinsic inclusion curvature (H_{m}). Within a reasonable range of model parameters, the numerical solutions obtained for the shape and inclusion density differ only little from the predictions obtained on the basis of the ADE model with effective model constants [Eq. (26)]. The effects of the inclusions can therefore be exactly described in this range of model parameters by the usual methods for treating the ADE model. If we calculate Δa and the corresponding shape within the limit of small single-inclusion energy for the values of parameters given in Fig. 1, we find that the results are almost identical to those obtained without expansion. However, the validity of the ADE approximation at a small total number of inclusions is guaranteed only provided that the principal curvatures are small over the whole membrane area and that H_{m} is small. From the expressions of the effective coefficients we can also estimate the importance of the value of inclusion curvature on the shape configuration. Thus, if we assume that $H_{\mathrm{m}} \ll 2k_{\mathrm{B}}T/\xi$, then the configurations obtained are almost independent of the inclusion curvature, as we can deduce from the effective coefficients. Otherwise, if we assume that $H_{\mathrm{m}} > 2k_{\mathrm{B}}T/\xi$, then the effect of H_{m} becomes significant since the corrections to the effective coefficients are proportional to the square of H_{m}.

In this work the effect of inclusions on vesicle shapes was analyzed only for a few specific examples. However, the obtained results can be extrapolated also to some other regions in the space of system parameters. For instance, in order to deduce the behavior of the oblate vesicle containing inclusions with negative intrinsic curvature as a function of the inclusion number, the behavior of the oblate vesicle at increasing the number of inclusions (Fig. 1) can be related to its behavior at increasing interaction constant (Fig. 6). Thus, if the inclusion curvature for the case presented in Fig. 1 were negative instead of positive, by increasing the inclusion number the corresponding configurations would involve narrow necks where the inclusion density significantly drops, similar to those presented in Fig. 6. Analogously, if the inclusion curvature for the case presented in Fig. 6 were positive instead of negative, configurations would be similar to those presented in Fig. 1 and at large interaction constants the shapes would be symmetric with respect to the equatorial plane.

It has to be borne in mind that it is the inclusions that induce the transition between different shape classes, as was shown here for the transition from a stomatocyte to a discocyte shape class (Fig. 1). It is reasonable to expect similar behavior also for other shape classes—e.g., that similar transitions occur between prolate shapes with and without equatorial mirror symmetry. The interdependence between the lateral distribution of the membrane constituents and the membrane shape plays an important role also in the undulated tubular shapes that are a subject of increasing interest [27,28]. It can be seen from the single-inclusion energy [Eq. (1)] that the inclusion which is characterized by its intrinsic principal curvatures is sensitive also to the Gaussian curvature (C_1C_2) which differs over the undulations and therefore modulates the single-inclusion energy and the free energy of inclusions even if the mean curvature of the membrane (H) were constant over the membrane. Thus, in our model the inclusions can induce a transformation of a cylindrical shape to the undulated shape. The transformation of the cylindrical shape to the undulated shape can also be understood on the basis of the expression for the effective coefficient of spontaneous curvature ($C_{0,\mathrm{eff}}$) from which it is evident that positive inclusion curvature causes the increase of $C_{0,\mathrm{eff}}$. It has been previously demonstrated that the increase of the spontaneous curvature induces the transformation into the undulated shapes [29].

Minimization of the total free energy [Eq. (5)] has been studied by parametric models which could predict the inclusion-initiated shape transitions from axially symmetric to nonaxisymmetric shapes [13]. It should nevertheless be stressed that the shapes obtained by using parametric models are in general restricted to a class of shapes defined by the chosen ansatz function. If the guessed ansatz is relevant, in that it is supported by the experimentally observed shapes, the parametric and rigorously obtained shapes differ primarily in that the exact solution yields a lower total energy than the parametric one. However, the parametric models, as our analysis shows, cannot predict the singular behavior of the system depicted in Figs. 2 and 3.

Our analysis revealed a singularity in the Euler-Lagrange system of equations, reflecting a possible discontinuity in the derivative of the lateral density of the inclusions and the derivative of the meridian principal curvature of an axisymmetric shape on the arclength (Fig. 3). The example presented in Fig. 2 showing the buildup of the singularity on increasing the relative area difference Δa illustrates the reasons for its occurrence based on the closeness of the vesicle membrane. The solution of the variational problem obtained in the vicinity of the Δa value at which the singularity occurs shows large variations of c_m and ν within a short region of the vesicle area. In our case of large h_m this behavior can be understood by the tendency of inclusions to accumulate in the regions of both poles where the mean curvatures are higher than in the vesicle middle. The inclusion lateral density is the highest at the pole with larger mean curvature. However, it is locally maximal also at the other pole and thus it decreases away from each pole of the vesicle to attain a minimum in the vesicle central region. There is also the tendency in the system to have the membrane area with curvatures favorable to inclusions as large as possible with the consequence that, at a given value of Δa, membrane curvatures around poles vary much less than in the case of a vesicle without inclusions (see Fig. 4). In accordance with this behavior, the lateral density of inclusions is decreasing towards the vesicle central region from both poles in a convex manner which makes it such that the matching can only occur within a small vesicle region. By increasing Δa, the increased mean principal curvatures at vesicle poles attract more and more inclusions to the pole regions, which makes the matching region in the vesicle middle narrower and narrower. The critical point occurs when this region becomes infinitely thin. A still further increase of Δa would lead to even larger mean curvatures at vesicle poles and more accumulated inclusions there, with the consequence that the inclusion lateral density could not be matched anymore in a derivable manner. Altogether, at given spontaneous curvature of the membrane and equilibrium area difference and a sufficiently strong interaction strength (ξ) together with the large number of inclusions (N_T), the lateral distribution of inclusions governed by the inclusion density in the vesicle pole cannot match anymore the lateral distribution governed by the inclusion density in the other vesicle pole. However, there is no phase separation up to the critical shape since the inclusion density is continuous. The discontinuity in $d\nu/dl$ is related to the discontinuity in the derivative of the meridian curvature [cf. Eq. (20)]. These effects, at a given interaction strength, are more pronounced in shapes that involve large values of principal curvatures at some vesicle locations. On the other hand, our calculations show (unpublished) that at increasing interaction strengths the singularity appears in shapes that do not involve large values of principal curvatures. It has to be pointed out that the generalization of the present model taking into account the direct interactions between the inclusions may smooth out the discontinuity in the derivative of the inclusion density in the critical shape.

The occurrence of the singular behavior described may have parallels in other related systems. Recently it was proposed, on the basis of theoretical study, that singular behavior exists also in one-component membrane vesicles in which the membrane constituents exhibit in-plane orientational ordering according to the local difference between the two principal membrane curvatures [25]. The same method of minimization of the membrane free energy that is used in this work was applied to the relevant free energy including the contribution of the orientational ordering and direct interactions between the membrane constituents. A critical shape occurred for some values of model parameters whereby the orientational distribution exhibited a sharp peak [25]. Both systems, membrane with inclusions and membrane consisting of building blocks that may undergo orientational ordering, involve energy contributions that are always negative, due to an additional "internal" degree of freedom. The singularity appears to occur when the effects due to this additional degree of freedom counterbalance the local isotropic bending [25].

The results presented in Figs. 1 and 2 show how the shape and lateral distribution of inclusions are coupled. Due to curvature-inclusion interaction the inclusions redistribute in an inhomogeneous manner which is against the entropy effect. The adjustments of the shape and lateral distribution of inclusions are such that the shape is changed in the direction to allow for a larger part of the vesicle membrane to have mean curvatures more favorable to inclusions and less membrane to have unfavorable mean curvatures, whereas the deviation of the lateral distribution of inclusions deviates less from the homogeneous distribution than in the case of an unadjusted shape [12,13]. The variational principle applied in our analysis assures us that the deviation of the lateral distribution of mobile membrane inclusions from the homogeneous distribution corresponds to the minimal free energy.

In conclusion, a rigorous treatment of the coupling of vesicle shape and lateral distribution of inclusions caused by a curvature-dependent membrane-inclusion interaction shows a nonlinear behavior expressed in specific shape modifications. It also shows the occurrence of a critical axisymmetric shape up to which the lateral density of membrane inclusions is continuous and derivable over the whole vesicle area.

[1] J. E. Rothman, Nature (London) **372**, 55 (1994).
[2] S. L. Schmid, Annu. Rev. Biochem. **66**, 511 (1997).
[3] J. Nance, BioEssays **27**, 126 (2005).
[4] S. Svetina and B. Žekš, J. Theor. Biol. **146**, 115 (1990).
[5] A. Iglič, M. Fošnarič, H. Hägerstrand, and V. Kralj-Iglič, FEBS Lett., **574**, 9 (2004).
[6] U. Seifert, Adv. Phys. **46**, 13 (1997); S. Svetina and B. Žekš, Anat. Rec., **268**, 215 (2002).
[7] J. L. Harden, F. C. MacKintosh, and P. D. Olmsted, Phys. Rev. E **72**, 11903 (2005).
[8] M. Goulian, Curr. Opin. Colloid Interface Sci., **1**, 358 (1996).
[9] D. R. Fattal and A. Ben-Shaul, Biophys. J. **65**, 1795 (1993); M. B. Partenskii and P. C. Jordan, J. Chem. Phys. **117**, 10768 (2002) (and references therein).
[10] V. S. Markin, Biophys. J. **36**, 1 (1981); S. Leibler, J. Phys. (Paris) **47**, 507 (1986); J. B. Fournier, Phys. Rev. Lett., **76**, 4436 (1996); D. Andelman, T. Kawakatsu, and K. Kawasaki, Europhys. Lett. **19**, 57 (1992).
[11] K. Bohinc, V. Kralj-Iglič, and S. May, J. Chem. Phys. **119**, 7435 (2003) (and references therein).
[12] S. Svetina, V. Kralj-Iglič, and B. Žekš, in *Biophysics of Membrane Transport*, Proceedings of the Tenth School, Szczyrk, Poland, 1990, edited by J. Kuczera and S. Przestalski (University of Wrocław, Poland, 1990), Vol. II, p. 139.
[13] V. Kralj-Iglič, S. Svetina, and B. Žekš, Eur. Biophys. J. **24**, 311 (1996).
[14] E. A. Evans, Biophys. J. **30**, 265 (1980); S. Svetina, M. Brumen, and B. Žekš, Stud. Biophys. **110**, 177 (1985); B. Božič, S. Svetina, B. Žekš, and R. E. Waugh, Biophys. J. **61**, 963 (1992); L. Miao, U. Seifert, M. Wortis, and H.-G. Döbereiner, Phys. Rev. E **49**, 5389 (1994).
[15] H. J. Deuling and W. Helfrich, J. Phys. (Paris) **37**, 1335 (1976); S. Svetina, and B. Žekš, Eur. Biophys. J. **17**, 101 (1989); U. Seifert, K. Berndl, and R. Lipowsky, Phys. Rev. A **44**, 1182 (1991).
[16] V. Kralj-Iglič, V. Heinrich, S. Svetina, and B. Žekš, Eur. Phys. J. B **10**, 5 (1999).
[17] A. Iglič and V. Kralj-Iglič, in *Planar Lipid Bilayers (BLMs) and Their Applications*, edited by H. T. Tien and A. Ottova-Leitmannova (Elsevier, Amsterdam, 2003), Vol. 7, p. 143.
[18] V. Kralj-Iglič, M. Remškar, M. Fošnarič, G. Vidmar, and A. Iglič, Phys. Lett. A **296**, 151 (2002); V. Kralj-Iglič, M. Remškar, and A. Iglič, in *Horizons in World Physics*, edited by A. Reimer (Nova Science, Hauppauge, NY, 2004), p. 111.
[19] M. Fošnarič, K. Bohinc, D. R. Gauger, A. Iglič, V. Kralj-Iglič, and S. May, J. Chem. Inf. Model **45**, 1652 (2005).
[20] E. A. Evans and R. Skalak, *Mechanics and Thermodynamics of Biomembranes* (CRC, Boca Raton, 1980).
[21] R. E. Waugh, J. Song, S. Svetina, and B. Žekš, Biophys. J. **61**, 974 (1992).
[22] K. Berndl, J. Käs, R. Lipowsky, E. Sackmann, and U. Seifert, Europhys. Lett. **13**, 659 (1990).
[23] M. Breidenich, R. R. Netz, and R. Lipowsky, Europhys. Lett. **49**, 431 (2000).
[24] D. Andelman, M. M. Kozlov, and W. Helfrich, Europhys. Lett. **25**, 231 (1994).
[25] V. Kralj-Iglič, B. Babnik, D. R. Gauger, S. May, and A. Iglič, J. Stat. Phys. (to be published).
[26] U. Seifert, Phys. Rev. Lett. **70**, 1335 (1993).
[27] T. Schemesh, A. Luini, V. Malhotra, K. N. J. Burger, and M. M. Kozlov, Biophys. J. **85**, 3813 (2003).
[28] A. Iglič, B. Babnik, U. Gimsa, and V. Kralj-Iglič, J. Phys. A **38**, 8527 (2005).
[29] B. Božič, V. Heinrich, S. Svetina, and B. Žekš, Eur. Phys. J. E **6**, 91 (2001).